IEEE Access
Multidisciplinary | Rapid Review | Open Access Journal

Received February 27, 2019, accepted March 13, 2019, date of publication March 15, 2019, date of current version April 3, 2019.

Digital Object Identifier 10.1109/ACCESS.2019.2905371

Finite-Time Super-Twisting Controller Based on SESO Design for RLV Re-Entry Phase

RONGJUN MU[1], JIAYE CHEN[1], KEKE PENG[2], XIN ZHANG[1], YANPENG DENG[1], AND NAIGANG CUI[1]

[1]School of Astronautics, Harbin Institute of Technology, Harbin 150001, China
[2]Harbin Jiancheng Group Company Ltd., Harbin 150030, China

Corresponding author: Jiaye Chen (flyhx13@163.com)

ABSTRACT In this paper, an improved extended state observer (ESO) based on sigmoid function and a finite-time convergence attitude controller are designed for reusable launch vehicle (RLV) in the re-entry phase. First, a control-oriented model (COM) of the RLV is established. According to the singular perturbation theory, the RLV control system is divided into an outer-loop and inner-loop subsystems. Second, a sigmoid function ESO (SESO) is proposed to estimate the model uncertainties and external disturbance caused by the large attitude maneuver and complicated external environment during the RLV re-entry phase. The continuous differentiable sigmoid function has the significant ability in noise suppression. By selecting the proper Lyapunov function, the stability of the SESO is proved. Then, based on the sliding mode control (SMC) theory, an improved multivariable super-twisting high-order sliding mode controller is designed. The finite-time convergence for the whole system is proven by the Lyapunov function technology. Finally, a 6-degree-of-freedom (6-DOF) RLV model is utilized to simulate to verify the effectiveness and robustness of the proposed control scheme.

INDEX TERMS Reusable launch vehicle, extended state observer, sliding mode control, super-twisting, re-entry phase.

I. INTRODUCTION

The research on reusable launch vehicle has received much attention because of its cost-efficient and reliable as an accessible approach to aerospace for both military and civilian application during the last few decades. During the re-entry phase, the RLV's velocity varies from Mach 20 to Mach 3, and it turns back with large attitude maneuver [1]. Therefore, a novel controller, which can be robust to the disturbance and uncertainty caused by bad flight condition, should be designed [2]. To sum up, the purpose of the RLV controller during the re-entry phase is to track the guidance command fast and accurately with the disturbance and model uncertainty.

During the past several years, many control algorithms have been applied to the RLV controller design during the re-entry phase, such as gain scheduling [3], nonlinear dynamic inversion [4], back-stepping control [5], and linear parameter varying [6], neural control [7], H-infinity control [8]. Although these control methods above can track the guidance command, the control ability is insufficient when the system exists severe uncertainty and external disturbance. Sliding mode control (SMC) has the significant advantage of dealing with the problems [9]. For the SMC, chattering is a problem need to be solved. Some techniques have been applied into SMC to fill the gap, such as adaptive law, disturbance observer and so on. In order to overcome the disadvantages of the conventional sliding mode reaching law, such as the large chattering and the slow convergence rate, an improved quick reaching law based on the global terminal sliding mode control is proposed for the unmanned surface vehicle in [10]. For solving the unsatisfactory control capability of a bearingless induction motor (BIM) under parameter variations, external disturbance, and load mutation, an adaptive exponential sliding mode controller and an extended sliding mode disturbance observer for on-line identification of system disturbance variables are designed in [11]. The stabilization is investigated about fuzzy stochastic singular systems by the use of sliding-mode control (SMC) in [12]. A sliding mode controller is developed in [13]

The associate editor coordinating the review of this manuscript and approving it for publication was Zheng Chen.

to assure tracking of guidance commands, and the interval type-2 fuzzy logic systems combined with adaptive technique are employed to approximate the nonlinear parts to improve the reentry attitude tracking performance. In [14], a novel controller called adaptive iterative learning sliding mode (AILSM) is developed to control linear and nonlinear fractional-order systems. Finite-time convergence control strategies based on adaptive non-singular fast terminal sliding mode are proposed for spacecraft attitude tracking subject to actuator faults, actuator saturation, external disturbances and inertia uncertainties [15]. To deal with the adaptive sliding-mode control problem for nonlinear active suspension systems via the Takagi-Sugeno (T-S) fuzzy approach [16]. A sliding mode control scheme in the framework of the back-stepping technique is designed in [17]. A novel finite-time controller which is derived using the bi-limit homogeneous technique for a system with both matched and mismatched disturbances is designed in [18]. In [19], a neural network (NN)-based multivariable fixed-time terminal sliding mode control (MFTTSMC) strategy for re-entry vehicles (RVs) with uncertainties is developed.

Recently, the high-order sliding mode (HOSM) control algorithm is carried out as a solution to attenuate the chattering [20]. One of the most widely used in HOSM method is the super-twisting algorithm (STA) [21]. Compared with other HOSM algorithm, STA does not employ sliding surface derivatives. A multivariable STA is proposed based on the STA, which has better feature [22]. A novel estimation for the upper bound of the super-twisting algorithm's reaching time the presence of perturbations is presented [23]. A gain-adaption mechanism of a dual level to the super-twisting algorithm (STA) for adaptive sliding mode design is studied in [24]. The development of two nonlinear robust higher-order flight control laws, a discontinuous sliding mode (DSM) control and super-twisting continuous control law, for roll-coupled maneuvers of fighter aircraft with uncertain parameters is discussed in [25]. Nagesh, Indira, and C. Edwards propose a multivariable super-twisting sliding mode structure which represents an extension of the well-known single input case [26]. The STA is also applied in the hypersonic vehicle in [27] and [28]. An adaptive super-twisting algorithm is incorporated with its observer counterpart on the system under consideration to get reliable attitude and vibration control in the presence of sensor noise and momentum coupling [29]. An adaptive twisting algorithm is proposed for systems subject to disturbances with unknown bounds and it can also avoid the aggressive chattering [30]. The RLV attitude model during the re-entry shows the obvious multivariable characteristic. A multivariable STA is well suited to solve the problem.

Disturbance observer based control is another important way to improve the disturbance suppression performance [31]. There are many nonlinear disturbance observers, such as sliding mode disturbance observer [11], high gain disturbance observer [32]. A uniform robust exact disturbance observer (UREDO) and a fixed-time controller for reusable launch vehicles are investigated in [33]. Extended state observer (ESO) as an important part of active disturbances rejection control proposed by Prof. Han, can estimate the state variables [34]. Combined with the reduced-order ESO, the approach of back-stepping and linear matrix inequality, an anti-disturbance controller is designed in [35]. Because of the sign function is used in the ESO, the output of ESO may not be smooth. In response to this issue, a sigmoid function is applied instead of sign function.

The key contributions of this paper are summarized as follows:

1) A sigmoid extended state observer (SESO) is designed. By using the sigmoid function instead of the sign function, the SESO has better application in the engineering;

2) A finite-time attitude controller based on multivariable super-twisting sliding mode is proposed. By using a fast terminal sliding mode manifold and a fast continuous super-twisting law, the controller can track the guidance attitude command accurately and efficiently, meanwhile attenuate the chattering.

The paper is organized as follows: the 6-DOF control-oriented model of RLV during the re-entry phase is established in Section II. Then the sigmoid extended state observer of the inner-loop and outer-loop subsystem is designed in Section III, and its estimation error is proved to converge to zero. Then, the multivariable super-twisting sliding mode controller of the inner-loop and outer-loop subsystem is proposed in Section IV, and it is proved to converge in finite time. Afterward, the simulation results are analyzed to verify the effectiveness of the control scheme in Section V. Finally, the conclusion is drawn in Section VI.

II. ATTITUDE MODELING OF RLV

During the re-entry flight phase, the RLV control system should track the attitude command accurately. The launch coordinate and the body coordinate are shown in Fig. 1.The origin o of the launch coordinate is selected as the launch position. ox points to the launch direction, oy points to the upwards vertical local level, and oz constitute the right hand system with ox, oy. The origin o_1 of the body coordinate is selected as the centroid of the RLV. o_1x_1 points to the forward direction of the body axis, o_1y_1 is in the symmetry plane of the RLV, and o_1z_1 constitute the right hand system with o_1x_1, o_1y_1. The RLV dynamics and kinematics model in the

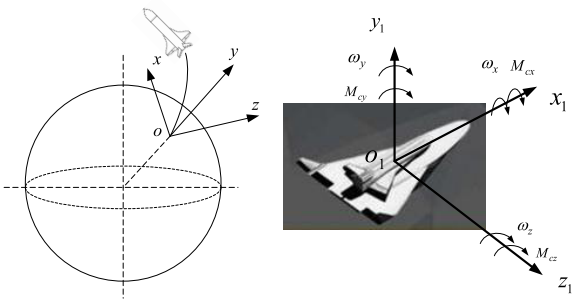

FIGURE 1. 6-DOF model of the rigid-body RLV.

re-entry phase is as follows, where the RLV is considered as a rigid body [1], [36]:

$$\begin{aligned}
\dot{\alpha} &= (\cos\theta\cos\gamma_v G - qSC_y^{\alpha}\alpha)/mV\cos\beta \\
&\quad - \tan\beta\cos\alpha\omega_x + \tan\beta\sin\alpha\omega_y + \omega_z \\
\dot{\beta} &= -(qSC_z^{\beta}\beta + \cos\theta\sin\gamma_v G)/mV \\
&\quad + \sin\alpha\omega_x + \cos\alpha\omega_y \\
\dot{\gamma} &= \omega_x + \tan\psi\sin\gamma\omega_y + \tan\psi\cos\gamma\omega_z \qquad (1) \\
\dot{\omega}_x &= [qSb(m_x^{\beta} + b(m_x^{\omega_y}\omega_y + m_x^{\omega_x}\omega_x)/2V) \\
&\quad - (J_z - J_y)\omega_y\omega_z]/J_x + M_{cx}/J_x \\
\dot{\omega}_y &= [qSb(m_y^{\beta} + b(m_y^{\omega_y}\omega_y + m_y^{\omega_x}\omega_x)/2V) \\
&\quad - (J_x - J_z)\omega_x\omega_z]/J_y + M_{cy}/J_y \\
\dot{\omega}_z &= [qSb(m_z^{\omega_z}\omega_z + m_z^{\alpha}\alpha)/2V - (J_y - J_x)\omega_x\omega_y]/J_z \\
&\quad + M_{cz}/J_z \qquad (2)
\end{aligned}$$

where α is the angle of attack(AOA); β is the sideslip angle; γ is the roll angle; θ is the trajectory inclination angle; γ_v is the bank angle; G represents the gravity of RLV; $q = \frac{1}{2}\rho V^2$ is the dynamic pressure; ρ is the air density; S is the reference area; m is the mass of RLV; V is the velocity of RLV; $\omega_x, \omega_y, \omega_z$ are the angular velocities of RLV's body coordinate rotation from launch coordinate respectively; ψ is the yaw angle; b is the reference length; M_{cx}, M_{cy}, M_{cz} are the control torques of the roll, yaw and pitch channel; $C_y^{\alpha}, C_z^{\beta}$ are the corresponding aerodynamic coefficients; $m_x^{\beta}, m_x^{\omega_y}, m_x^{\omega_x}, m_y^{\beta}, m_y^{\omega_y}, m_y^{\omega_x}, m_z^{\omega_z}, m_z^{\alpha}$ are the aerodynamic moment coefficients; $\boldsymbol{J} = \mathrm{diag}(J_x, J_y, J_z)$ is the mass inertia matrix of the vehicle.

In equation (1) and (2), there are strong nonlinearity and coupling between different channels, that bring difficulties for the attitude controller design. Thus, a control-oriented model (COM) [1] is established based on the following assumptions: 1) since the translational motion is much slower than the rotational motion of the RLV, the translational terms in the rotational equations can be set to zero; 2) since the RLV is much faster than Earth in rotational motion, the angular velocity of Earth can be neglected. Based on the two assumptions, the COM can be obtained as follows:

$$\begin{aligned}
\dot{\boldsymbol{\Omega}} &= \boldsymbol{R}\boldsymbol{\omega} + \boldsymbol{\Delta f} \\
\dot{\boldsymbol{\omega}} &= \boldsymbol{J}_0^{-1}\boldsymbol{\Phi}\boldsymbol{J}_0\boldsymbol{\omega} + \boldsymbol{J}_0^{-1}\boldsymbol{M} + \Delta\boldsymbol{d} \qquad (3)
\end{aligned}$$

where $\boldsymbol{\Omega} = [\alpha, \beta, \gamma]^T$ is the attitude angular vector, $\boldsymbol{\omega} = [\omega_x, \omega_y, \omega_z]^T$ is the angular velocity vector, $\boldsymbol{M} = [M_{cx}, M_{cy}, M_{cz}]^T$ is the control torque vector, $\boldsymbol{\Delta f}$ is the model uncertainty vector caused by the simplification and the influence of channel coupling, and $\Delta\boldsymbol{d}$ is the external disturbance torque vector. The matrix $\boldsymbol{R}$, $\boldsymbol{J}_0$, and $\boldsymbol{\Phi}$ are as follows:

$$\boldsymbol{R} = \begin{bmatrix} -\tan\beta\cos\alpha & \tan\beta\sin\alpha & 1 \\ \sin\alpha & \cos\alpha & 0 \\ 1 & \tan\psi\sin\gamma & \tan\psi\cos\gamma \end{bmatrix}$$

$$\boldsymbol{J}_0 = \begin{bmatrix} J_x & 0 & 0 \\ 0 & J_y & 0 \\ 0 & 0 & J_z \end{bmatrix}, \quad \boldsymbol{\Phi} = \begin{bmatrix} 0 & \omega_z & -\omega_y \\ -\omega_z & 0 & \omega_x \\ \omega_y & -\omega_x & 0 \end{bmatrix}.$$

III. SIGMOID EXTENDED STATE OBSERVER

According to singular perturbation theory, RLV control system is divided into outer-loop and inner-loop subsystems. The control system scheme is shown in Fig. 2:

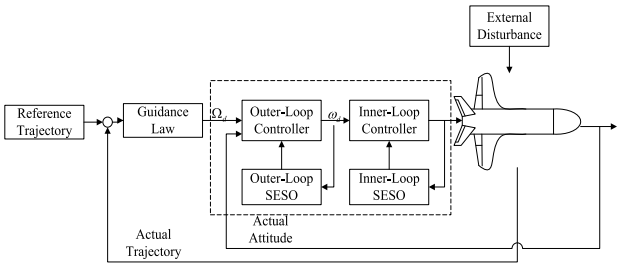

FIGURE 2. The finite-time control scheme for RLV.

A. OUTER-LOOP SESO DESIGN

Considering the COM of the RLV during the re-entry phase in equation (3), the sigmoid extended state observer (SESO) is designed to estimate the model uncertainties and external disturbance.

It is assumed that the derivative of the model uncertainty vector is bounded, i.e. $\|\boldsymbol{\Delta}\dot{\boldsymbol{f}}\| \le \varpi_1$, $\varpi_1 > 0$. Define the error variables:

$$\begin{cases} z_1 = \boldsymbol{\Omega} - \boldsymbol{\Omega}_d \\ z_2 = \boldsymbol{\omega} - \boldsymbol{\omega}_d \end{cases} \qquad (4)$$

Then the SESO of the outer-loop subsystem is designed as follows:

$$\begin{cases} \dot{\bar{z}}_{11} = \boldsymbol{R}\boldsymbol{\omega} - \dot{\boldsymbol{\Omega}}_d + \bar{z}_{12} - \boldsymbol{\beta}_{s1}\mathrm{sigm}(\boldsymbol{E}_{11}; \boldsymbol{E}_{11a}, \boldsymbol{E}_{11b}) \\ \dot{\bar{z}}_{12} = -\boldsymbol{\beta}_{s2}\mathrm{sigm}(\boldsymbol{E}_{11}; \boldsymbol{E}_{11a}, \boldsymbol{E}_{11b}) \end{cases} \qquad (5)$$

where $\boldsymbol{E}_{11} = \bar{z}_{11} - z_1$, $\boldsymbol{E}_{11} \in \mathbb{R}^{3\times1}$, $\bar{z}_{11} \in \mathbb{R}^{3\times1}$, $\boldsymbol{\beta}_{s1}$ and $\boldsymbol{\beta}_{s2}$ are parameters to be designed, $\mathrm{sigm}(\boldsymbol{E}_{11}; \boldsymbol{E}_{11a}, \boldsymbol{E}_{11b})$ is the sigmoid function. The sigmoid function is defined as $\mathrm{sigm}(x) = \mathrm{sigm}(x; a, b) = a[(1+e^{-bx})^{-1} - 0.5]$. To simplify, the $\mathrm{sigm}(\boldsymbol{E}_{11}; \boldsymbol{E}_{11a}, \boldsymbol{E}_{11b})$ is recorded as $\mathrm{sigm}(\boldsymbol{E}_{11})$ in the following derivation process.

By selecting the observer parameters $\boldsymbol{\beta}_{s1}$ and $\boldsymbol{\beta}_{s2}$ appropriately, the extended state $\bar{z}_{12}$ will approach $\boldsymbol{\Delta f}$. The parameters need to design is shown in Table 1.

TABLE 1. Range of parameters.

Parameter	Range
$\boldsymbol{E}_{11a}$	$E_{11a} > 2\sqrt{\left(\frac{4\varpi_1\sqrt{4I+\beta_{s1}^2}}{\beta_{s2}\lambda_{\min}(\boldsymbol{Q}_{SESO})}\right)^2 - \mathrm{sigm}^2(\boldsymbol{E}_{11})}$
$\boldsymbol{E}_{11b}$	$\boldsymbol{E}_{11b} = \boldsymbol{\beta}_{s2}/\boldsymbol{\varepsilon}$
$\boldsymbol{\beta}_{s1}$	$0 < \boldsymbol{\beta}_{s1} < \sqrt{8\sqrt{2}+12}\boldsymbol{I}$
$\boldsymbol{\beta}_{s2}$	$\boldsymbol{\beta}_{s2} > 0$

Theorem 1: Considering the SESO of equation (5), if the extended state $\dot{\bar{z}}_{12}$ is unknown but bounded, the parameters

$$\boldsymbol{E}_{11a} > 2\sqrt{(\frac{4\boldsymbol{\varpi}_1\sqrt{4\boldsymbol{I}+\boldsymbol{\beta}_{s1}^2}}{\boldsymbol{\beta}_{s2}\boldsymbol{\lambda}_{\min}(\boldsymbol{Q}_{SESO})})^2 - \mathrm{sigm}^2(\boldsymbol{E}_{11})},$$

$\boldsymbol{E}_{11b} = \boldsymbol{\beta}_{s2}/\boldsymbol{\varepsilon}, 0 < \boldsymbol{\beta}_{s1} < \sqrt{8\sqrt{2}+12}\boldsymbol{I}, \boldsymbol{\varepsilon} > 0, \boldsymbol{\beta}_{s2} > 0$, the observation vector error will converge to zero.

Proof: Define $\boldsymbol{E}_{12} = \bar{z}_{12} - \Delta\boldsymbol{f}$, combine equation (4) and equation (5), the error dynamic system can be written as:

$$\begin{cases} \dot{\boldsymbol{E}}_{11} = \boldsymbol{E}_{12} - \boldsymbol{\beta}_{s1}\mathrm{sigm}(\boldsymbol{E}_{11}) \\ \dot{\boldsymbol{E}}_{12} = -\boldsymbol{\beta}_{s2}\mathrm{sigm}(\boldsymbol{E}_{11}) - \Delta\dot{\boldsymbol{f}} \end{cases} \tag{6}$$

Selecting the Lyapunov function as:

$$\begin{aligned} \boldsymbol{L}_{11} &= \mathrm{sigm}^2(\boldsymbol{E}_{11}) + (\frac{\boldsymbol{\beta}_{s1}}{2}\mathrm{sigm}(\boldsymbol{E}_{11}) - \boldsymbol{E}_{12})^2 \\ &= (\frac{\boldsymbol{\beta}_{s1}^2}{4}+1)\mathrm{sigm}^2(\boldsymbol{E}_{11}) + E_{12}^2 - \boldsymbol{\beta}_{s1}\mathrm{sigm}(\boldsymbol{E}_{11})\boldsymbol{E}_{12} \\ &= \boldsymbol{\kappa}^T\boldsymbol{P}_{SESO}\boldsymbol{\kappa} \end{aligned} \tag{7}$$

where $\boldsymbol{\kappa} = [\mathrm{sigm}(\boldsymbol{E}_{11}; \boldsymbol{E}_{11a}, \boldsymbol{E}_{11b}), \boldsymbol{E}_{12}]^T$,

$$\boldsymbol{P}_{SESO} = \frac{1}{2}\begin{bmatrix} \frac{\boldsymbol{\beta}_{s1}^2}{2}+2 & -\boldsymbol{\beta}_{s1} \\ -\boldsymbol{\beta}_{s1} & 2 \end{bmatrix}.$$

The derivative of the sigmoid function is:

$$\frac{d[\mathrm{sigm}(\boldsymbol{E}_{11})]}{dt} = [\frac{\boldsymbol{E}_{11b}}{\boldsymbol{E}_{11a}}(\frac{1}{4}\boldsymbol{E}_{11a}^2 - \mathrm{sigm}^2(\boldsymbol{E}_{11}))]\dot{\boldsymbol{E}}_{11} \tag{8}$$

The derivative of equation (7) is:

$$\begin{aligned} \dot{\boldsymbol{L}}_{11} = {} & 2(\frac{\boldsymbol{\beta}_{s1}^2}{4}+1)\mathrm{sigm}(\boldsymbol{E}_{11})\frac{\boldsymbol{E}_{11b}}{\boldsymbol{E}_{11a}}(\frac{1}{4}\boldsymbol{E}_{11a}^2 \\ & -\mathrm{sigm}^2(\boldsymbol{E}_{11}))\dot{\boldsymbol{E}}_{11} + 2\boldsymbol{E}_{12}\dot{\boldsymbol{E}}_{12} - \boldsymbol{\beta}_{s1}\frac{\boldsymbol{E}_{11b}}{\boldsymbol{E}_{11a}}(\frac{1}{4}\boldsymbol{E}_{11a}^2 \\ & -\mathrm{sigm}^2(\boldsymbol{E}_{11}))\dot{\boldsymbol{E}}_{11}\boldsymbol{E}_{12} - \boldsymbol{\beta}_{s1}\,\mathrm{sigm}(\boldsymbol{E}_{11})\dot{\boldsymbol{E}}_{12} \end{aligned} \tag{9}$$

It can be obtained by substituting equation (6) into equation (9) that:

$$\begin{aligned} \dot{\boldsymbol{L}}_{11} = {} & (-\frac{\boldsymbol{\varepsilon}}{4}\boldsymbol{E}_{11b}\boldsymbol{\beta}_{s1}^3 - \boldsymbol{\varepsilon}\boldsymbol{E}_{11b}\boldsymbol{\beta}_{s1} + \boldsymbol{\beta}_{s1}\boldsymbol{\beta}_{s2})\mathrm{sigm}^2(\boldsymbol{E}_{11}) \\ & +(\frac{\boldsymbol{\varepsilon}}{2}\boldsymbol{E}_{11b}\boldsymbol{\beta}_{s1}^2 - 2\boldsymbol{\beta}_2 + \frac{\boldsymbol{\varepsilon}}{4}\boldsymbol{\beta}_{s1}^2\boldsymbol{E}_{11b} \\ & +\boldsymbol{\varepsilon}\boldsymbol{E}_{11b})\mathrm{sigm}(\boldsymbol{E}_{11})\boldsymbol{E}_{12} - \boldsymbol{\beta}_{s1}\frac{\boldsymbol{\varepsilon}}{2}\boldsymbol{E}_{11b}\boldsymbol{E}_{12}^2 - 2\boldsymbol{E}_{12}\boldsymbol{\varpi}_1 \\ & +\boldsymbol{\beta}_{s1}\mathrm{sigm}(\boldsymbol{E}_{11})\boldsymbol{\varpi}_1 \end{aligned} \tag{10}$$

where $\boldsymbol{\varepsilon} = -\frac{\boldsymbol{\beta}_{s1}^2+4\boldsymbol{I}-\boldsymbol{E}_{11a}^2}{2\boldsymbol{E}_{11a}}$, and $\boldsymbol{E}_{11b} = \boldsymbol{\beta}_{s2}\boldsymbol{\varepsilon}^{-1}$, then:

$$\dot{\boldsymbol{L}}_{11} = -\frac{1}{4}\boldsymbol{\beta}_{s2}\boldsymbol{\kappa}^T\boldsymbol{Q}_{SESO}\boldsymbol{\kappa} + \boldsymbol{\varpi}_1\bar{\mathbf{B}}\boldsymbol{\kappa} \tag{11}$$

where $\boldsymbol{Q}_{SESO} = \frac{1}{2}\begin{bmatrix} 2\boldsymbol{\beta}_{s1}^3 & 4\boldsymbol{I}-3\boldsymbol{\beta}_{s1}^2 \\ 4\boldsymbol{I}-3\boldsymbol{\beta}_{s1}^2 & 4\boldsymbol{\beta}_{s1} \end{bmatrix}, \bar{\mathbf{B}} = \begin{bmatrix} \boldsymbol{\beta}_{s1} \\ -2\boldsymbol{I} \end{bmatrix}^T$.

To ensure that $\boldsymbol{Q}_{SESO} > 0$, then $0 < \boldsymbol{\beta}_{s1} < \sqrt{8\sqrt{2}+12}\boldsymbol{I}$. Then:

$$\begin{aligned} \dot{\boldsymbol{L}}_{11} &= -\frac{1}{4}\boldsymbol{\beta}_{s2}\boldsymbol{\kappa}^T\boldsymbol{Q}_{SESO}\boldsymbol{\kappa} + \boldsymbol{\varpi}_1\sqrt{4\boldsymbol{I}+\boldsymbol{\beta}_{s1}^2}\boldsymbol{\kappa} \\ &\le -(\frac{1}{4}\boldsymbol{\beta}_{s2}\boldsymbol{\lambda}_{\min}(\boldsymbol{Q}_{SESO})\,\|\boldsymbol{\kappa}\|_2 - \boldsymbol{\varpi}\sqrt{4\boldsymbol{I}+\boldsymbol{\beta}_{s1}^2})\,\|\boldsymbol{\kappa}\|^2 \end{aligned} \tag{12}$$

If $\boldsymbol{\beta}_{s2}\boldsymbol{\lambda}_{\min}(\boldsymbol{Q}_{SESO})\,\|\boldsymbol{\kappa}\|_2/4\boldsymbol{I} > \boldsymbol{\varpi}_1\sqrt{4\boldsymbol{I}+\boldsymbol{\beta}_{s1}^2}$, then $\dot{\boldsymbol{L}}_{11} < 0$, which shows that the error converges. For $\|\boldsymbol{\kappa}\|_2^2 = \mathrm{sigm}^2(\boldsymbol{E}_{11}) + \boldsymbol{E}_{12}^2$, $sigm^2(\boldsymbol{E}_{11}) \le \boldsymbol{E}_{11a}^2/4\boldsymbol{I}$, then:

$$\begin{aligned} |\boldsymbol{E}_{12}| &= \sqrt{\|\boldsymbol{\kappa}\|_2^2 - \mathrm{sigm}^2(\boldsymbol{E}_{11})} \\ &\le \sqrt{(\frac{4\boldsymbol{\varpi}_1\sqrt{4\boldsymbol{I}+\boldsymbol{\beta}_{s1}^2}}{\boldsymbol{\beta}_{s2}\boldsymbol{\lambda}_{\min}(\boldsymbol{Q}_{SESO})})^2 - \mathrm{sigm}^2(\boldsymbol{E}_{11})} \end{aligned} \tag{13}$$

Choosing the Lyapunov function as $\boldsymbol{L}_{12} = \frac{1}{2}\boldsymbol{E}_{11}\boldsymbol{E}_{11}^T$, its derivative is as follow:

$$\begin{aligned} \dot{\boldsymbol{L}}_{12} &= \boldsymbol{E}_{11}\dot{\boldsymbol{E}}_{11} = -\boldsymbol{\beta}_{s1}\boldsymbol{E}_{11}\,\mathrm{sigm}(\boldsymbol{E}_{11}) + \boldsymbol{E}_{11}\boldsymbol{E}_{12} \\ &\le -\boldsymbol{\beta}_{s1}\boldsymbol{E}_{11}\mathrm{sigm}(\boldsymbol{E}_{11}) \\ &\quad + |\boldsymbol{E}_{11}|\sqrt{(\frac{4\boldsymbol{\varpi}_1\sqrt{4\boldsymbol{I}+\boldsymbol{\beta}_{s1}^2}}{\boldsymbol{\beta}_{s2}\boldsymbol{\lambda}_{\min}(\boldsymbol{Q}_{SESO})})^2 - \mathrm{sigm}^2(\boldsymbol{E}_{11})} \end{aligned} \tag{14}$$

For $\mathrm{sigm}(\boldsymbol{E}_{11}) \in (-0.5\boldsymbol{E}_{11a}, 0.5\boldsymbol{E}_{11a})$, then select proper $\boldsymbol{\beta}_{s1}$ that makes:

$$\|\boldsymbol{\beta}_{s1}\mathrm{sigm}(\boldsymbol{E}_{11})\| > \sqrt{(\frac{4\boldsymbol{\varpi}_1\sqrt{4\boldsymbol{I}+\boldsymbol{\beta}_{s1}^2}}{\boldsymbol{\beta}_{s2}\boldsymbol{\lambda}_{\min}(\boldsymbol{Q}_{SESO})})^2 - \mathrm{sigm}^2(\boldsymbol{E}_{11})}$$

Then $\dot{\boldsymbol{L}}_{12} < 0$, i.e. $\dot{\boldsymbol{L}}_{12}$ is negative definite. ■

B. INNER-LOOP SESO DESIGN

According to the similar design method above, suppose that $\|\Delta\boldsymbol{d}\| \le \boldsymbol{\varpi}_2, \boldsymbol{\varpi}_2 > 0$, then the SESO of the inner-loop can be obtained as:

$$\begin{cases} \dot{\bar{z}}_{21} = \boldsymbol{J}_0^{-1}\boldsymbol{\Phi}\boldsymbol{J}_0\omega - \omega_d + \bar{z}_{22} - \boldsymbol{\beta}_{f1}\mathrm{sigm}(\boldsymbol{E}_{21}) \\ \dot{\bar{z}}_{22} = -\boldsymbol{\beta}_{f2}\mathrm{sigm}(\boldsymbol{E}_{21}) \end{cases} \tag{15}$$

where $\boldsymbol{E}_{21} = \bar{z}_{21} - z_2$ is the estimation error. According to Theorem 1, if the parameters $\boldsymbol{\beta}_{f1}, \boldsymbol{\beta}_{f2}$ are selected properly, the extended state $\bar{z}_{22}$ will converge to $\Delta\boldsymbol{d}$.

IV. MULTIVARIABLE SUPER-TWISTING SLIDING MODE CONTROLLER DESIGN

The attitude guidance command is $\boldsymbol{\Omega}_d$, and the angular velocity guidance command is $\boldsymbol{\omega}_d$, the attitude tracking error is:

$$\boldsymbol{e}_\Omega = \boldsymbol{\Omega} - \boldsymbol{\Omega}_d \tag{16}$$

The derivative of (16) is:

$$\dot{\boldsymbol{e}}_\Omega = \dot{\boldsymbol{\Omega}} - \dot{\boldsymbol{\Omega}}_d = \boldsymbol{R}\boldsymbol{\omega} + \Delta\boldsymbol{f} - \dot{\boldsymbol{\Omega}}_d \tag{17}$$

The derivative of (17) is:

$$\ddot{\boldsymbol{e}}_\Omega = \ddot{\boldsymbol{\Omega}} - \ddot{\boldsymbol{\Omega}}_d = \boldsymbol{R}\boldsymbol{J}_0^{-1}\boldsymbol{\Phi}\boldsymbol{J}_0\boldsymbol{\omega} - \ddot{\boldsymbol{\Omega}}_d + \boldsymbol{R}\boldsymbol{J}_0^{-1}\boldsymbol{M} + \boldsymbol{D} \tag{18}$$

where $\boldsymbol{D} = \dot{\boldsymbol{R}}\boldsymbol{\omega} + \boldsymbol{R}\Delta\boldsymbol{d} + \Delta\dot{\boldsymbol{f}}$.

The angular velocity tracking error is:

$$\boldsymbol{e}_\omega = \boldsymbol{\omega} - \boldsymbol{\omega}_d \tag{19}$$

The derivative of (19) is:

$$\dot{\boldsymbol{e}}_\omega = \dot{\boldsymbol{\omega}} - \dot{\boldsymbol{\omega}}_d = \boldsymbol{J}_0^{-1}\boldsymbol{\Phi}\boldsymbol{J}_0\boldsymbol{\omega} + \boldsymbol{J}_0^{-1}\boldsymbol{M} + \Delta\boldsymbol{d} - \dot{\boldsymbol{\omega}}_d \tag{20}$$

A. OUTER-LOOP CONTROLLER DESIGN

Choosing the super-twisting sliding mode surface as:

$$\boldsymbol{s}_\Omega = \boldsymbol{e}_\Omega + k_\Omega \int_0^t \mathrm{sn}^{\gamma_\Omega}(\boldsymbol{e}_\Omega)d\tau \tag{21}$$

where $\mathrm{sn}^{\gamma}(\boldsymbol{e}) = [|e_1|^{\gamma}\,\mathrm{sat}(e_1), |e_2|^{\gamma}\,\mathrm{sat}(e_2), |e_3|^{\gamma}\,\mathrm{sat}(e_3)]^T$, $k_\Omega > 0$, $0 < \gamma_\Omega < 1$. Define the saturation function as follows:

$$\mathrm{sat}(s) = \begin{cases} 1, & s > \varepsilon \\ s/\varepsilon, & |s| < \varepsilon \\ -1, & s < -\varepsilon. \end{cases}$$

Differentiating equation(21), we can get:

$$\begin{aligned} \dot{\boldsymbol{s}}_\Omega &= \dot{\boldsymbol{e}}_\Omega + k_\Omega \mathrm{sn}^{\gamma_\Omega}(\boldsymbol{e}_\Omega) \\ &= R\boldsymbol{\omega} - \boldsymbol{\Omega}_d + \Delta\boldsymbol{f} + k_\Omega \mathrm{sn}^{\gamma_\Omega}(\boldsymbol{e}_\Omega) \end{aligned} \tag{22}$$

To weaken the chattering and reach the sliding mode manifold fast, a novel multivariable super-twisting control law is designed as follows [9], [26]:

$$\begin{aligned} \dot{\boldsymbol{s}}_\Omega &= -k_{\Omega 1}\frac{\boldsymbol{s}_\Omega}{\|\boldsymbol{s}_\Omega\|^{1/2}} - k_{\Omega 2}\boldsymbol{s}_\Omega + \boldsymbol{\chi}_\Omega \\ \dot{\boldsymbol{\chi}}_\Omega &= -k_{\Omega 3}\frac{\boldsymbol{s}_\Omega}{\|\boldsymbol{s}_\Omega\|} - k_{\Omega 4}\boldsymbol{s}_\Omega \end{aligned} \tag{23}$$

where $\boldsymbol{\chi}_\Omega$ is an auxiliary variable vector. Substituting equation (23) into equation (22), the control law can be obtained as:

$$\begin{aligned} \boldsymbol{\omega}_c &= \boldsymbol{R}^{-1}[-\dot{\boldsymbol{\Omega}}_d - k_\Omega \mathrm{sn}^{\gamma_\Omega}(\boldsymbol{e}_\Omega) - k_{\Omega 1}\frac{\boldsymbol{s}_\Omega}{\|\boldsymbol{s}_\Omega\|^{1/2}} \\ &\quad -k_{\Omega 2}\boldsymbol{s}_\Omega - \Delta\hat{\boldsymbol{f}} + \boldsymbol{\chi}_\Omega] \\ \dot{\boldsymbol{\chi}}_\Omega &= -k_{\Omega 3}\frac{\boldsymbol{s}_\Omega}{\|\boldsymbol{s}_\Omega\|} - k_{\Omega 4}\boldsymbol{s}_\Omega \end{aligned} \tag{24}$$

Theorem 2: Considering the nonlinear system (3), assume that $\boldsymbol{v} = \dot{\boldsymbol{R}}\boldsymbol{e}_\omega + \dot{\boldsymbol{e}}_f$ satisfies $\|\boldsymbol{v}\| \le \delta_1 \|\boldsymbol{s}\|$, $\delta_1 > 0$. If the control law is designed as equation (24), there exist certain values for $k, k_{\Omega 1}, \ldots, k_{\Omega 4}$ and γ_Ω that makes the tracking error $\boldsymbol{e}_\Omega$ converge to zero in finite time.

Proof: Substituting equation (24) to (22), it can be obtained that:

$$\begin{aligned} \dot{s}_\Omega &= -k_{\Omega 1}\frac{s_\Omega}{\|s_\Omega\|^{1/2}} - k_{\Omega 2}s_\Omega + \boldsymbol{\chi}_\Omega + \boldsymbol{v} \\ \dot{\chi}_\Omega &= -k_{\Omega 3}\frac{s_\Omega}{\|s_\Omega\|} - k_{\Omega 4}s_\Omega \end{aligned} \tag{25}$$

Selecting the Lyapunov function as:

$$\boldsymbol{V}_s = 2k_{\Omega 3}\|\boldsymbol{s}_\Omega\| + k_{\Omega 4}\boldsymbol{s}_\Omega^T\boldsymbol{s}_\Omega + \frac{1}{2}\boldsymbol{\chi}_\Omega^T\boldsymbol{\chi}_\Omega + \frac{1}{2}\boldsymbol{\zeta}^T\boldsymbol{\zeta} \tag{26}$$

where $\boldsymbol{\zeta} = k_{\Omega 1}\frac{\boldsymbol{s}_\Omega}{\|\boldsymbol{s}_\Omega\|^{1/2}} + k_{\Omega 2}\boldsymbol{s}_\Omega - \boldsymbol{\chi}_\Omega$.

Differentiating equation (26):

$$\begin{aligned} \dot{\boldsymbol{V}}_s &= \left(\frac{1}{2}k_{\Omega 1}^2 + 2k_{\Omega 3}\right)\frac{\boldsymbol{s}_\Omega^T\dot{\boldsymbol{s}}_\Omega}{\|\boldsymbol{s}_\Omega\|} + \left(k_{\Omega 2}^2 + 2k_{\Omega 4}\right)\boldsymbol{s}_\Omega^T \\ &\quad +2\boldsymbol{\chi}_\Omega^T\dot{\boldsymbol{\chi}}_\Omega + \frac{3}{2}k_{\Omega 1}k_{\Omega 2}\frac{\boldsymbol{s}_\Omega^T\dot{\boldsymbol{s}}_\Omega}{\|\boldsymbol{s}_\Omega\|^{1/2}} - k_{\Omega 2}(\dot{\boldsymbol{s}}_\Omega^T\boldsymbol{\chi}_\Omega \\ &\quad +\boldsymbol{s}_\Omega^T\dot{\boldsymbol{\chi}}_\Omega) - k_{\Omega 1}\left[\frac{\dot{\boldsymbol{\chi}}_\Omega^T\boldsymbol{s}_\Omega + \boldsymbol{\chi}_\Omega^T\dot{\boldsymbol{s}}_\Omega}{\|\boldsymbol{s}_\Omega\|^{1/2}} - \frac{1}{2}\frac{(\boldsymbol{s}_\Omega^T\dot{\boldsymbol{s}}_\Omega)(\boldsymbol{\chi}_\Omega^T\boldsymbol{s}_\Omega)}{\|\boldsymbol{s}_\Omega\|^{5/2}}\right] \end{aligned} \tag{27}$$

Substituting $\boldsymbol{\chi}_\Omega$, $\boldsymbol{\zeta}_\Omega$ into equation (27):

$$\begin{aligned} &\dot{\boldsymbol{V}}_s \\ &= -\left(k_{\Omega 1}k_{\Omega 3} + \frac{1}{2}k_1^3\right)\|\boldsymbol{s}_\Omega\|^{1/2} - \left(k_{\Omega 2}k_{\Omega 3} + 2k_{\Omega 1}^2k_{\Omega 2}\right)\|\boldsymbol{s}_\Omega\| \\ &\quad -\left(k_{\Omega 2}^3 + k_{\Omega 2}k_{\Omega 4}\right)\|\boldsymbol{s}_\Omega\|^2 - \left(\frac{5}{2}k_{\Omega 1}k_{\Omega 2}^2 + k_{\Omega 1}k_{\Omega 4}\right)\|\boldsymbol{s}_\Omega\|^{3/2} \\ &\quad + k_{\Omega 1}^2\frac{\boldsymbol{s}_\Omega^T\boldsymbol{\chi}_\Omega}{\|\boldsymbol{s}_\Omega\|} + 2k_{\Omega 2}^2\boldsymbol{s}_\Omega^T\boldsymbol{\chi}_\Omega + 3k_{\Omega 1}k_{\Omega 2}\frac{\boldsymbol{s}_\Omega^T\boldsymbol{\chi}_\Omega}{\|\boldsymbol{s}_\Omega\|^{1/2}} \\ &\quad - k_{\Omega 2}\|\boldsymbol{\chi}_\Omega\|^2 + \frac{1}{2}k_{\Omega 1}\frac{(\boldsymbol{s}_\Omega^T\boldsymbol{\chi}_\Omega)(\boldsymbol{\chi}_\Omega^T\boldsymbol{s}_\Omega)}{\|\boldsymbol{s}_\Omega\|^{5/2}} - k_{\Omega 1}\frac{\boldsymbol{\chi}_\Omega^T\boldsymbol{\chi}_\Omega}{\|\boldsymbol{s}_\Omega\|^{1/2}} \\ &\quad + \left(\frac{1}{2}k_{\Omega 1}^2 + 2k_{\Omega 3}\right)\frac{\boldsymbol{s}_\Omega^T\boldsymbol{v}}{\|\boldsymbol{s}_\Omega\|} + \left(k_{\Omega 2}^2 + 2k_{\Omega 4}\right)\boldsymbol{s}_\Omega^T\boldsymbol{v} \\ &\quad + \frac{3}{2}k_{\Omega 1}k_{\Omega 2}\frac{\boldsymbol{s}_\Omega^T\boldsymbol{v}}{\|\boldsymbol{s}_\Omega\|^{1/2}} + \frac{1}{2}k_{\Omega 1}\frac{(\boldsymbol{s}_\Omega^T\boldsymbol{v})(\boldsymbol{\chi}_\Omega^T\boldsymbol{s}_\Omega)}{\|\boldsymbol{s}_\Omega\|^{5/2}} \\ &\quad - k_{\Omega 1}\frac{\boldsymbol{\chi}_\Omega^T\boldsymbol{v}}{\|\boldsymbol{s}_\Omega\|^{1/2}} - k_{\Omega 2}\boldsymbol{v}^T\boldsymbol{\chi}_\Omega \end{aligned} \tag{28}$$

According to the Cauchy-Schwarz inequality, the equation (28) can be transformed to:

$$\begin{aligned} \dot{\boldsymbol{V}}_s \le &-\left(k_{\Omega 1}k_{\Omega 3} + \frac{1}{2}k_1^3\right)\|\boldsymbol{s}_\Omega\|^{1/2} - \left(k_{\Omega 2}k_{\Omega 3} + 2k_{\Omega 1}^2k_{\Omega 2}\right)\|\boldsymbol{s}_\Omega\| \\ &-\left(k_{\Omega 2}^3 + k_{\Omega 2}k_{\Omega 4}\right)\|\boldsymbol{s}_\Omega\|^2 - \left(\frac{5}{2}k_{\Omega 1}k_{\Omega 2}^2 + k_{\Omega 1}k_{\Omega 4}\right)\|\boldsymbol{s}_\Omega\|^{3/2} \\ &+ k_{\Omega 1}^2\frac{\left|\boldsymbol{s}_\Omega^T\boldsymbol{\chi}_\Omega\right|}{\|\boldsymbol{s}_\Omega\|} + 2k_{\Omega 2}^2\left|\boldsymbol{s}_\Omega^T\boldsymbol{\chi}_\Omega\right| + 3k_{\Omega 1}k_{\Omega 2}\frac{\left|\boldsymbol{s}_\Omega^T\boldsymbol{\chi}_\Omega\right|}{\|\boldsymbol{s}_\Omega\|^{1/2}} \\ &- k_{\Omega 2}\|\boldsymbol{\chi}_\Omega\|^2 + \frac{1}{2}k_{\Omega 1}\frac{\left|\boldsymbol{s}_\Omega^T\boldsymbol{\chi}_\Omega\right|^2}{\|\boldsymbol{s}_\Omega\|^{5/2}} + k_{\Omega 1}\frac{\|\boldsymbol{\chi}_\Omega\|^2}{\|\boldsymbol{s}_\Omega\|^{1/2}} \\ &+ \left(\frac{1}{2}k_{\Omega 1}^2 + 2k_{\Omega 3}\right)\frac{\left|\boldsymbol{s}_\Omega^T\boldsymbol{v}\right|}{\|\boldsymbol{s}_\Omega\|} + \left(k_{\Omega 2}^2 + 2k_{\Omega 4}\right)\left|\boldsymbol{s}_\Omega^T\boldsymbol{v}\right| \\ &+ \frac{3}{2}k_{\Omega 1}k_{\Omega 2}\frac{\left|\boldsymbol{s}_\Omega^T\boldsymbol{v}\right|}{\|\boldsymbol{s}_\Omega\|^{1/2}} + \frac{1}{2}k_{\Omega 1}\frac{\left|\boldsymbol{s}_\Omega^T\boldsymbol{v}\right|\left|\boldsymbol{\chi}_\Omega^T\boldsymbol{s}_\Omega\right|}{\|\boldsymbol{s}_\Omega\|^{5/2}} \\ &+ k_{\Omega 1}\frac{\left|\boldsymbol{\chi}_\Omega^T\boldsymbol{v}\right|}{\|\boldsymbol{s}_\Omega\|^{1/2}} + k_{\Omega 2}\left|\boldsymbol{v}^T\boldsymbol{\chi}_\Omega\right| \end{aligned} \tag{29}$$

With the bound of $\|\boldsymbol{v}\| \leq \delta_1 \|\boldsymbol{s}\|$, the equation (29) can be converted to:

$$\begin{aligned}
&\dot{\boldsymbol{V}}_s \\
&\leq -\left(k_{\Omega 1}k_{\Omega 3}+\frac{1}{2}k_1^3\right)\|\boldsymbol{s}_\Omega\|^{1/2}-\left(k_{\Omega 2}k_{\Omega 3}+2k_{\Omega 1}^2k_{\Omega 2}\right)\|\boldsymbol{s}_\Omega\| \\
&\quad -\left(k_{\Omega 2}^3+k_{\Omega 2}k_{\Omega 4}\right)\|\boldsymbol{s}_\Omega\|^2-\left(\frac{5}{2}k_{\Omega 1}k_{\Omega 2}^2+k_{\Omega 1}k_{\Omega 4}\right)\|\boldsymbol{s}_\Omega\|^{3/2} \\
&\quad +k_{\Omega 1}^2\frac{\left|\boldsymbol{s}_\Omega^T\boldsymbol{\chi}_\Omega\right|}{\|\boldsymbol{s}_\Omega\|}+2k_{\Omega 2}^2\left|\boldsymbol{s}_\Omega^T\boldsymbol{\chi}_\Omega\right|+3k_{\Omega 1}k_{\Omega 2}\frac{\left|\boldsymbol{s}_\Omega^T\boldsymbol{\chi}_\Omega\right|}{\|\boldsymbol{s}_\Omega\|^{1/2}} \\
&\quad -k_{\Omega 2}\|\boldsymbol{\chi}_\Omega\|^2+\frac{1}{2}k_{\Omega 1}\frac{\left|\boldsymbol{s}_\Omega^T\boldsymbol{\chi}_\Omega\right|^2}{\|\boldsymbol{s}_\Omega\|^{5/2}}+k_{\Omega 1}\frac{\|\boldsymbol{\chi}_\Omega\|^2}{\|\boldsymbol{s}_\Omega\|^{1/2}} \\
&\quad +\left(\frac{1}{2}k_{\Omega 1}^2+2k_{\Omega 3}\right)\delta_1\|\boldsymbol{s}_\Omega\|+\left(k_{\Omega 2}^2+2k_{\Omega 4}\right)\delta_1\|\boldsymbol{s}_\Omega\|^2 \\
&\quad +\frac{3}{2}k_{\Omega 1}k_{\Omega 2}\delta_1\|\boldsymbol{s}_\Omega\|^{3/2}+\frac{3}{2}k_{\Omega 1}\delta_1\|\boldsymbol{s}_\Omega\|^{1/2}\|\boldsymbol{\chi}_\Omega\| \\
&\quad +k_{\Omega 2}\delta_1\|\boldsymbol{s}_\Omega\|\|\boldsymbol{\chi}_\Omega\| \qquad (30)
\end{aligned}$$

Define $\boldsymbol{X}=\left[\|\boldsymbol{s}_\Omega\|^{1/2},\boldsymbol{s}_\Omega,\boldsymbol{\chi}_\Omega\right]^{\boldsymbol{T}}$, then:

$$\dot{\boldsymbol{V}}_s \leq -\frac{1}{\|\boldsymbol{s}_\Omega\|^{1/2}}\boldsymbol{X}^T\boldsymbol{P}\boldsymbol{X}-X^T\boldsymbol{Q}\boldsymbol{X} \qquad (31)$$

where $\boldsymbol{P},\boldsymbol{Q}$ are as follows:

$$P=\begin{bmatrix}P_{11}&0&P_{13}\\0&P_{22}&P_{23}\\P_{31}&P_{32}&P_{33}\end{bmatrix}\text{ with the elements are:}$$

$$\begin{aligned}
P_{11}&=\frac{1}{2}k_{\Omega 1}^3+k_{\Omega 1}k_{\Omega 3}\\
P_{13}&=-\frac{1}{2}k_{\Omega 1}^2\\
P_{22}&=k_{\Omega 1}k_{\Omega 4}+\frac{5}{2}k_{\Omega 2}^2k_{\Omega 1}-\frac{3}{2}k_{\Omega 1}k_{\Omega 2}\delta_1\\
P_{23}&=-\frac{3}{2}k_{\Omega 1}k_{\Omega 2}\\
P_{31}&=P_{13}\\
P_{32}&=P_{23}\\
P_{33}&=\frac{1}{2}k_{\Omega 1}
\end{aligned}$$

$$\boldsymbol{Q}=\begin{bmatrix}Q_{11}&0&Q_{13}\\0&Q_{22}&Q_{23}\\Q_{31}&Q_{32}&Q_{33}\end{bmatrix}\text{ with the elements are:}$$

$$\begin{aligned}
Q_{11}&=k_{\Omega 2}k_{\Omega 3}+2k_{\Omega 1}^2k_{\Omega 2}-\left(\frac{1}{2}k_{\Omega 1}^2+2k_{\Omega 3}\right)\delta_1\\
Q_{13}&=-\frac{3}{4}k_{\Omega 1}\delta_1\\
Q_{22}&=k_{\Omega 2}k_{\Omega 4}+k_{\Omega 2}^3-(k_{\Omega 2}^2+2k_{\Omega 4})\delta_1\\
Q_{23}&=-k_{\Omega 2}^2-\frac{1}{2}k_{\Omega 2}\delta_1\\
Q_{31}&=Q_{13}\\
Q_{32}&=Q_{23}\\
Q_{33}&=k_{\Omega 2}
\end{aligned}$$

In order to make $\boldsymbol{P}>0$ and $\boldsymbol{Q}>0$ satisfied simultaneously, the parameters are selected as:

$$\begin{cases}
k_{\Omega 1}>0\\
k_{\Omega 2}>2\delta_1\\
k_{\Omega 3}>\dfrac{\frac{9}{16}(k_{\Omega 1}\delta_1)^2}{k_{\Omega 2}(k_{\Omega 2}-2\delta_1)}+\dfrac{\frac{1}{2}k_{\Omega 1}^2\delta_1-2k_{\Omega 1}^2k_{\Omega 2}}{k_{\Omega 2}-2\delta_1}\\
k_{\Omega 4}>\dfrac{\left(1.5k_{\Omega 1}^2k_{\Omega 2}+3\delta_1k_{\Omega 2}\right)^2}{k_{\Omega 1}^2k_{\Omega 3}-2\delta_1^2-3\delta_1k_{\Omega 1}^2}+2k_{\Omega 2}^2
\end{cases} \qquad (32)$$

From equation (31), by utilizing the Rayleigh's inequality, it can be obtained that:

$$\dot{\boldsymbol{V}}_s \leq -\frac{1}{\|\boldsymbol{s}_\Omega\|^{1/2}}\boldsymbol{X}^T\boldsymbol{P}\boldsymbol{X} \leq -\frac{1}{\|\boldsymbol{s}_\Omega\|^{1/2}}\lambda_{\min}(P)\|\boldsymbol{X}\|^2 \qquad (33)$$

Define $\varsigma=[\frac{\boldsymbol{s}_\Omega}{\|\boldsymbol{s}_\Omega\|^{1/2}},\boldsymbol{s}_\Omega,\boldsymbol{\chi}_\Omega]^T$, and it is obvious that $\|\boldsymbol{X}\|=\|\varsigma\|$. Thus the equation (33) can be written as: $\dot{\boldsymbol{V}}_s \leq -\frac{1}{\|\boldsymbol{s}_\Omega\|^{1/2}}\lambda_{\min}(P)\|\varsigma\|^2$. The Lyapunov function of equation (26) can be rewritten as:

$$\boldsymbol{V}_s=\varsigma^T\boldsymbol{\Xi}\varsigma \leq \lambda_{\max}(\boldsymbol{\Xi})\|\varsigma\|^2 \qquad (34)$$

where the symmetric positive-definite matrix $\boldsymbol{\Xi}$ is:

$$\boldsymbol{\Xi}=\frac{1}{2}\begin{bmatrix}4k_{\Omega 3}+k_{\Omega 1}^2&k_{\Omega 1k_{\Omega 2}}&-k_{\Omega 1}\\k_{\Omega 1}k_{\Omega 2}&2k_{\Omega 4+k_{\Omega 2}^2}&-k_{\Omega 2}\\-k_{\Omega 1}&-k_{\Omega 2}&2\end{bmatrix}.$$

Thus the equation (33) can be transferred to the following form:

$$\dot{\boldsymbol{V}}_s \leq -\frac{1}{\|\boldsymbol{s}_\Omega\|^{1/2}}\lambda_{\min}(\boldsymbol{P})\|\boldsymbol{X}\|^2 \leq -\frac{1}{\|\boldsymbol{s}_\Omega\|^{1/2}}\frac{\lambda_{\min}(P)}{\lambda_{\max}(\boldsymbol{\Xi})}\boldsymbol{V}_s \qquad (35)$$

Then $V_s \leq -\sigma V_s^{1/2}$, where $\sigma=\frac{\lambda_{\min}(\boldsymbol{P})\sqrt{\lambda_{\min}(\boldsymbol{\Xi})}}{\lambda_{\max}(\boldsymbol{\Xi})}$.

It can be concluded that if the parameters $k_{\Omega 1},\ldots,k_{\Omega 4}$ are selected appropriately, $\boldsymbol{s}_\Omega$ and its derivative can converge to zero in finite time $t_{s_\Omega} \leq \frac{2V_s^{1/2}(0)}{\sigma}$ [23].

Afterward, to make $\dot{\boldsymbol{s}}_\Omega$ converge to zero, that is:

$$\dot{\boldsymbol{e}}_\Omega+k\mathrm{sig}^{\gamma_\Omega}(\boldsymbol{e}_\Omega)=0 \qquad (36)$$

Choosing the positive-definite Lyapunov function:

$$\boldsymbol{V}_e=\frac{1}{2}\boldsymbol{e}_\Omega^T\boldsymbol{e}_\Omega=\frac{1}{2}\sum_{i=1}^{3}\boldsymbol{e}_i^2 \qquad (37)$$

The derivative of equation (37) is:

$$\begin{aligned}
\dot{\boldsymbol{V}}_e&=\sum_{i=1}^{3}e_i\dot{e}_i=-k_\Omega\sum_{i=1}^{3}\mathrm{sn}^{\gamma_\Omega}e_i=-k_\Omega\sum_{i=1}^{3}|e_i|^{\gamma_\Omega}\\
&\leq -k_\Omega\sum_{i=1}^{3}|e_i|^{\gamma_\Omega+1} \leq -k_\Omega\left(\sum_{i=1}^{3}e_i^2\right)^{\frac{\gamma_\Omega+1}{2}}=-k_\Omega V_e^{\frac{\gamma_\Omega+1}{2}}
\end{aligned} \qquad (38)$$

From the above in equation, if the parameters k_Ω, γ_Ω are selected properly, $\boldsymbol{e}_\Omega$ can converge to zero in finite time $t_{e_\Omega} \leq \frac{\|e_{(0)}\|^{1-\gamma_\Omega}}{(1-\gamma_\Omega)k}$. Some details can be found in [23].

Finally, $\boldsymbol{e}_\Omega$ can converge to zero in $t_\Omega = t_{s_\Omega} + t_{\boldsymbol{e}_\Omega}$. ■

B. INNER-LOOP CONTROLLER DESIGN

The inner-loop controller is to design the control torque $\boldsymbol{M}$ to make $\boldsymbol{\omega}$ tracking the guidance command $\boldsymbol{\omega}_d$, considering the external disturbance $\Delta\boldsymbol{d}$.

Considering the design method of the outer-loop, the fast terminal sliding mode manifold is defined as:

$$\boldsymbol{s}_\omega = \boldsymbol{e}_\omega + k_\omega \int_0^t \mathrm{sn}^{\gamma_\omega}(\boldsymbol{e}_\omega) d\tau \tag{39}$$

where $k_\omega > 0$, $0 < \gamma_\omega < 1$.

The derivate of the above equation is:

$$\dot{\boldsymbol{s}}_\omega = \boldsymbol{J}_0^{-1}\boldsymbol{\Phi}\boldsymbol{J}_0\boldsymbol{\omega} + \boldsymbol{J}_0^{-1}\boldsymbol{M} + \Delta\boldsymbol{d} - \dot{\boldsymbol{\omega}}_d + k_\omega \mathrm{sn}^{\gamma_\omega}(\boldsymbol{e}_\omega) \tag{40}$$

Substituting the equation (40) into the equation (23), the control law can be obtained as follows:

$$\begin{aligned} \boldsymbol{M} &= \boldsymbol{J}_0[\boldsymbol{J}_0^{-1}\boldsymbol{\Phi}\boldsymbol{J}_0\boldsymbol{\omega} - k_\omega \mathrm{sn}^{\gamma_\omega}(\boldsymbol{e}_\omega) - k_{\omega 1}\frac{\boldsymbol{s}_\omega}{\|\boldsymbol{s}_\omega\|^{1/2}} \\ &\quad - k_{\omega 2}\boldsymbol{s}_\omega - \Delta\boldsymbol{d} + \boldsymbol{\chi}_\omega] \\ \dot{\boldsymbol{\chi}}_\omega &= -k_{\omega 3}\frac{\boldsymbol{s}_\omega}{\|\boldsymbol{s}_\omega\|} - k_{\omega 4}\boldsymbol{s}_\omega \end{aligned} \tag{41}$$

According to the proof of the Theorem 2, if the parameters $k_\omega, k_{\omega 1}, \ldots, k_{\omega 4}$ and γ_ω are selected properly, $\boldsymbol{s}_\omega, \dot{\boldsymbol{s}}_\omega$ will converge to zero in finite time t_{s_ω}, and $\boldsymbol{e}_\omega$ converges to zero in finite time t_{e_ω}. Hence, $\boldsymbol{e}_\omega$ can converge to zero in $t_\omega = t_{s_\omega} + t_{e_\omega}$.

V. SIMULATION ANALYZE

This section presents the simulation and results analysis of the proposed control scheme. In order to verify the effectiveness of the SESO proposed in Section III, according to [8], a compared ESO based on the super-twisting algorithm is designed as follows:

$$\begin{cases} \dot{\bar{z}}_{11} = \boldsymbol{R}\boldsymbol{\omega} - \dot{\boldsymbol{\Omega}}_d + \bar{z}_{12} - \boldsymbol{\beta}_{z1}\mathrm{sign}^{(a+1)/2}(z_{11} - \bar{z}_{11}) \\ \qquad -\boldsymbol{\beta}_{z2}(z_{11} - \bar{z}_{11}) \\ \dot{\bar{z}}_{12} = -\boldsymbol{\beta}_{z3}\mathrm{sign}^{a}(z_{11} - \bar{z}_{11}) - \boldsymbol{\beta}_{z4}(z_{11} - \bar{z}_{11}) \end{cases} \tag{42}$$

Change the multi-variable system (5), (42) to three same structure SISO system, and choose one system to verify the performances of the two kinds of ESO. The parameters of the super-twisting extended state observer (STESO) are selected as $\beta_{z1} = 5, \beta_{z2} = 20, \beta_{z3} = 1.5, \beta_{z4} = 150, a = 0.5$. The parameters of the SESO are selected as $\beta_{s1} = 4, \beta_2 = 18, E_{11a} = 2, E_{11b} = 18$, and the actual disturbance is set as:

$$\Delta f = \begin{cases} 0 & 0 \leq t < 10 \\ \cos(20) & 10 \leq t < 20 \\ \cos(t) & t > 20, \end{cases}$$

The simulation result is shown in Fig. 3. The result shows that both the STESO and SESO can estimate the disturbance.

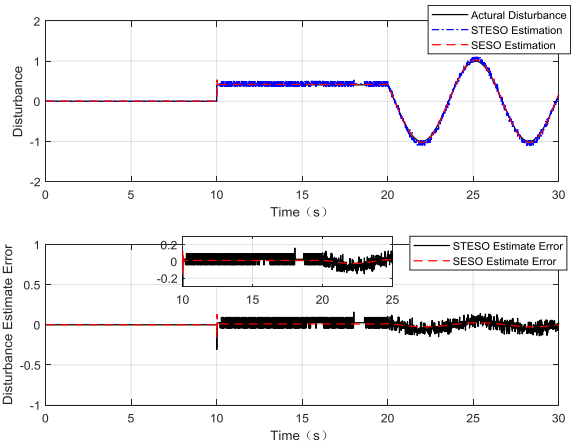

FIGURE 3. The STESO, SESO estimation results.

The maximum estimation errors of the two observers are listed in Table 2. However, for the SESO utilizes the sigmoid function instead of sign function, the SESO estimation error is lower than the STESO, and the STESO has more parameters to regulate without clear adjustment rules, the SESO is more suitable for engineering application.

TABLE 2. The maximum estimation errors of the two observers.

STESO	SESO
-0.3081	0.1292

Select the 6-DOF RLV during the re-entry phase as the simulation model. The initial simulation conditions are set as follows: the initial attitude of the re-entry phase is $\boldsymbol{\Omega}_0 = [51.2452°, -2.0498°, 180°]$, the initial angular velocity is $\omega_0 = [0, 0, 0](\mathrm{deg}/s)$, the RLV trajectory is shown in Fig. 4, the re-entry flight time is set as 500s, the step size is set as

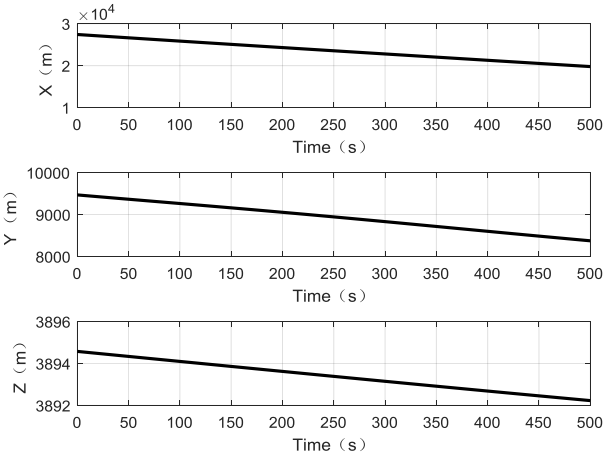

FIGURE 4. The RLV trajectory.

0.01s, the moment of inertia is:

$$\boldsymbol{J}_0 = \begin{bmatrix} 56241 & 0 & 0 \\ 0 & 10^6 & 0 \\ 0 & 0 & 985392 \end{bmatrix} \text{kg} \cdot \text{m}^2,$$

and the control parameters are set as Table 3. Inspired by the controller proposed by [1], the compared controller is consist of the controller of [1] and the STESO proposed by equation (42).

TABLE 3. Value of parameters.

Parameter	Value
k_Ω	2
$k_{\Omega 1}$	2
$k_{\Omega 2}$	4
$k_{\Omega 3}$	1
$k_{\Omega 4}$	0.5
γ_Ω	1.5
k_ω	15
$k_{\omega 1}$	5
$k_{\omega 2}$	4.5
$k_{\omega 3}$	0.2
$k_{\omega 4}$	0.2
γ_ω	1.5

The simulation results are shown in Fig. 5-Fig. 9.

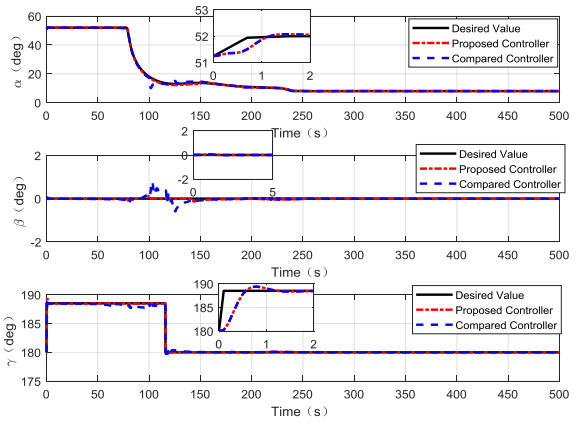

FIGURE 5. The attitude of controllers.

Fig. 5-Fig. 6 show the attitude $\boldsymbol{\Omega}$ tracking curves and the tracking errors of the proposed controller and the compared controller. The compared controller is a finite-time super-twisting controller based on the STESO. The maximum errors are shown in the Table 4. It can be seen that the maximum errors of the proposed controller are 1.028°, 0.18°, 0.89°, while the maximum errors of the compared controller are 7.2°, 0.8°, 1°. That's because the SESO can estimate the external disturbance and model uncertainties more precisely and compensate them. It is obvious that the big attitude of RLV happens during 77s - 150s, and by using the super-twisting algorithm, the proposed controller can effectively suppress the chattering, while the compared controller has

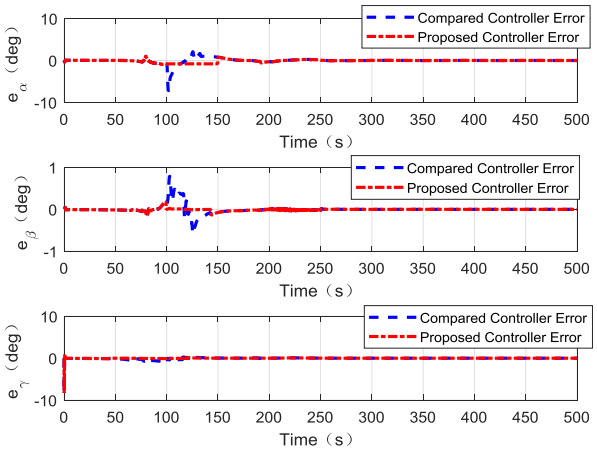

FIGURE 6. Attitude tracking errors of controllers.

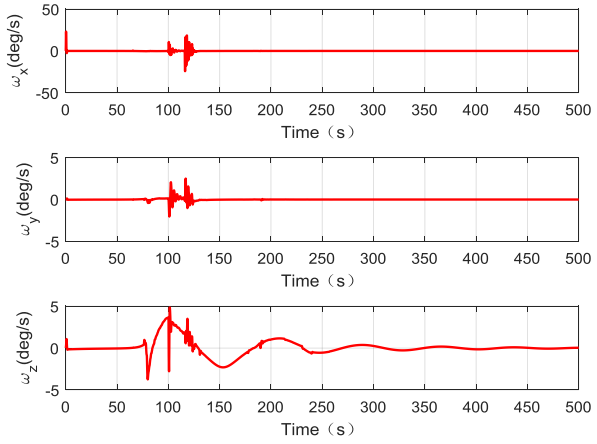

FIGURE 7. Angular velocities of the proposed controller.

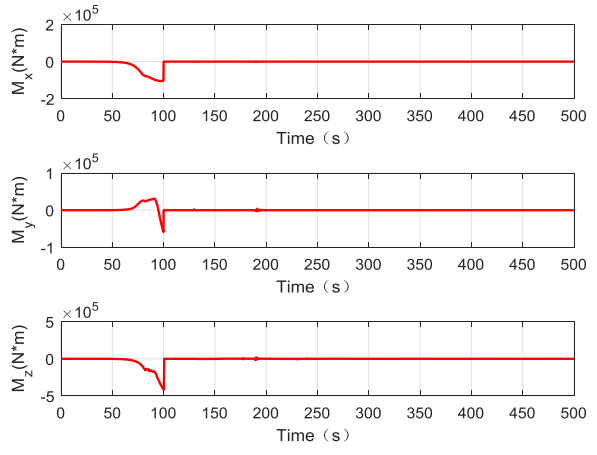

FIGURE 8. Control torques of the proposed controller.

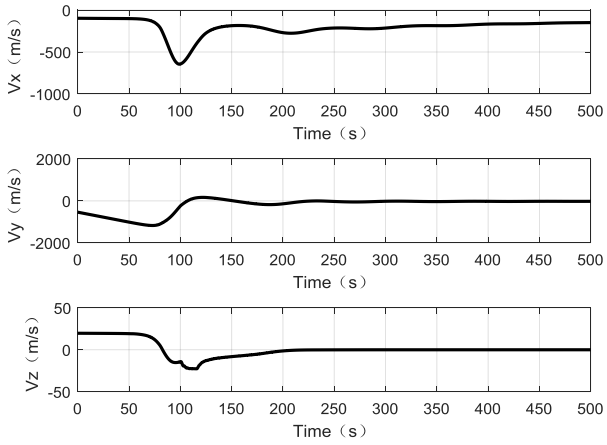

FIGURE 9. Velocities of the proposed controller.

TABLE 4. Attitude angle maximum errors of the two controller.

Attitude angle	Proposed Controller	Compared Controller
α	1.028°	7.2°
β	0.18°	0.8°
γ	0.89°	1°

larger error and chattering. That's because the proposed controller can reach the sliding manifold fast. The proposed outer-loop subsystem controller can converge in 1.6s.

The attitude angular velocities are shown in Fig. 7. From that, it can be observed that the maximum angular velocities are -24.18deg/s, 2.504deg/s, 4.859deg/s. When the RLV has big attitude change during 77s-150s, the chattering is small and acceptable. The proposed inner-loop subsystem controller can converge in 1.8s.

Fig. 8 shows the control torque during the re-entry phase of the RLV. It is obvious that the maximum control torque is less than 4×10^5(N*m), which is lower than the maximum torque that the RLV can provide.

Fig. 9 shows the velocities of the RLV during the re-entry phase. From the simulation results, it can be obviously seen that the curves of the velocity are smooth without big chattering. From that we can see that the proposed controller has good ability in chattering suppression.

From the simulation result, we can draw the conclusion that the controller proposed in this paper can track the guidance command rapidly and precisely.

VI. CONCLUSION

In this paper, a novel controller is designed based on the SESO to track the guidance command in finite time during the RLV re-entry phase considering the model uncertainties and external disturbances. The SESO is able to estimate the uncertainties and disturbances precisely and rapidly for the nonlinear RLV system. By applying the sigmoid function instead of the sign function in the ESO, the outputs of the ESO become smooth. The controller based on the multivariable finite-time super-twisting sliding mode control can converge in finite time and effectively suppressing the chattering simultaneously. The simulation results verify the effectiveness and advantages of the control scheme.

The future work will be that an improved adaptive disturbance observer should be studied to deal with the circumstance that if the bounds of model uncertainty and external disturbance are not known.

REFERENCES

[1] Q. Dong, Q. Zong, B. Tian, and F. Wang, "Integrated finite-time disturbance observer and controller design for reusable launch vehicle in reentry phase," *J. Aerosp. Eng.*, vol. 30, no. 1, pp. 1–11, 2017. doi: 10.1061/(ASCE)AS.1943-5525.0000670.

[2] Q. Dong, Q. Zong, B. Tian, and F. Wang, "Adaptive-gain multivariable super-twisting sliding mode control for reentry RLV with torque perturbation," *Int. J. Robust Nonlinear Control*, vol. 27, pp. 620–638, Mar. 2016. doi: 10.1002/rnc.3589.

[3] G. Wei, Z. Wang, W. Li, and L. Ma, "A survey on gain-scheduled control and filtering for parameter-varying systems," *Discrete Dyn. Nature Soc.*, vol. 2014, Apr. 2014, Art. no. 105815. doi: 10.1155/2014/105815.

[4] J. Sung, "Nonlinear Dynamic Inversion Control Law Development of High Performance Fighter Aircraft," *J. Inst. Control, Robot. Syst.*, vol. 23, no. 9, pp. 786–802, 2017. doi: 10.5302/J.ICROS.2017.17.0075.

[5] X. Shao and H. Wang, "Back-stepping robust trajectory linearization control for hypersonic reentry vehicle via novel tracking differentiator," *J. Franklin Inst.*, vol. 353, no. 9, pp. 1957–1984, Jun. 2016. doi: 10.1016/j.jfranklin.2016.03.007.

[6] M. M. Morato, D. J. Regner, P. R. C. Mendes, J. E. Normey-Rico, and C. Bordons, "Fault analysis, detection and estimation for a microgrid via H_2/H∞ LPV Observers," *Int. J. Electr. Power Energy Syst.*, vol. 105, pp. 823–845, Feb. 2019. doi: 10.1016/j.ijepes.2018.09.018.

[7] X. Wang, X. Yin, and F. Shen, "Robust adaptive neural tracking control for a class of nonlinear systems with unmodeled dynamics using disturbance observer," *Neurocomputing*, vol. 291, pp. 49–62, May 2018. doi: 10.1016/j.neucom.2018.02.082.

[8] Q. Mao, L. Dou, Q. Zong, and Z. Ding, "Attitude controller design for reusable launch vehicles during reentry phase via compound adaptive fuzzy H-infinity control," *Aerosp. Sci. Technol.*, vol. 72, pp. 36–48, Jan. 2018. doi: 10.1016/j.ast.2017.10.012.

[9] A. Levant, "Robust exact differentiation via sliding mode technique," *Automatica*, vol. 34, no. 3, pp. 379–384, Mar. 1998. 10.1016/S0005-1098(97)00209-4.

[10] X. Chunbo and P. Guo, "Global terminal sliding mode control with the quick reaching law and its application," *IEEE Access*, vol. 6, pp. 49793–49800, 5 Sep. 2018. doi: 10.1109/ACCESS.2018.2868785.

[11] Z. Yang, D. Zhang, X. Sun, and X. Ye, "Adaptive exponential sliding mode control for a bearingless induction motor based on a disturbance observer," *IEEE Access*, vol. 6, pp. 35425–35434, Jun. 2018. doi: 10.1109/ACCESS.2018.2851590.

[12] Z. Qingling, J. Zhang, and Y. Wang, "Robust sliding-mode control for fuzzy stochastic singular systems with different local input matrices," *IEEE Access*, vol. 6, pp. 29391–29406, May 2018. doi: 10.1109/ACCESS.2018.2837063.

[13] Q. Mao, L. Dou, B. Tian, and Q. Zong, "Reentry attitude control for a reusable launch vehicle with aeroservoelastic model using type-2 adaptive fuzzy sliding mode control," *Int. J. Robust Nonlinear Control*, vol. 28, no. 18, pp. 5858–5875, Dec. 2018. doi: 10.1002/rnc.4349.

[14] E. G. Razmjou, S. K. H. Sani, and J. Sadati, "Robust adaptive sliding mode control combination with iterative learning technique to output tracking of fractional-order systems," *Trans. Inst. Meas. Control*, vol. 40, no. 6, pp. 1808–1818, Apr. 2018. doi: 10.1177/0142331217691337.

[15] Z. Han, K. Zhang, T. Yang, and M. Zhang, "Spacecraft fault-tolerant control using adaptive non-singular fast terminal sliding mode," *IET Control Theory Appl.*, vol. 10, no. 16, pp. 1991–1999, Oct. 2016. doi: 10.1049/iet-cta.2016.0044.

[16] H. Li, J. Yu, C. Hilton, and H. Liu, "Adaptive sliding-mode control for nonlinear active suspension vehicle systems using T–S fuzzy approach," *IEEE Trans. Ind. Electron.*, vol. 60, no. 8, pp. 3328–3338, Aug. 2013. doi: 10.1109/TIE.2012.2202354.

[17] F. Wang, Q. Zou, C. Hua, and Q. Zong, "Finite-time attitude tracking control design for reusable launch vehicle in reentry phase based on disturbance observer," *Adv. Mech. Eng.*, vol. 9, no. 12, pp. 1–13, Dec. 2017. doi: 10.1177/1687814017744077.
[18] B. Tian, H. Lu, Z. Zuo, and Q. Zong, "Multivariable uniform finite-time output feedback reentry attitude control for RLV with mismatched disturbance," *J. Franklin Inst.*, vol. 355, no. 8, pp. 3470–3487, May 2018. doi: 10.1016/j.jfranklin.2018.01.042.
[19] X. Wang, J. Guo, and S. Tang, "Neural network-based multivariable fixed-time terminal sliding mode control for re-entry vehicles," *IET Control Theory Appl.*, vol. 12, no. 12, pp. 1763–1772, Aug. 2018. doi: 10.1049/iet-cta.2017.1309.
[20] A. Levant, "Sliding order and sliding accuracy in sliding mode control," *Int. J. Control*, vol. 58, no. 6, pp. 1247–1263, Dec. 1993. doi: 10.1080/00207179308923053.
[21] S. Kamal, A. Sachan, D. K. Kumar, and D. Singh, "Robust finite time cooperative control of second order agents: A multi-input multi-output higher order super-twisting based approach," *ISA Trans.*, vol. 86, pp. 1–8, Nov. 2018. doi: 10.1016/j.isatra.2018.10.041.
[22] R. Seeber, M. Reichhartinger, and M. Horn, "A Lyapunov function for an extended super-twisting algorithm," *IEEE Trans. Autom. Control*, vol. 63, no. 10, pp. 3426–3433, Oct. 2018. doi: 10.1109/TAC.2018.2794411.
[23] R. Seeber, M. Horn, and L. Fridman , "A novel method to estimate the reaching time of the super-twisting algorithm," *IEEE Trans. Autom. Control*, vol. 63, no. 12, pp. 4301–4308, Dec. 2018. doi: 10.1109/TAC.2018.2812789.
[24] L. Dong, X. Xiong, S. Jin, and S. Kamal, "Adaptive gains of dual level to super-twisting algorithm for sliding mode design," *IET Control Theory Appl.*, vol. 12, no. 17, pp. 2347–2356, Nov. 2018. doi: 10.1049/iet-cta.2018.5380.
[25] K. Raj, V. Muthukumar, S. N. Singh, and K. W. Lee, "Finite-time sliding mode and super-twisting control of fighter aircraft," *Aerosp. Sci. Technol.*, vols. 82–83, pp. 487–498, Nov. 2018. doi: 10.1016/j.ast.2018.09.028.
[26] I. Nagesh and C. Edwards, "A multivariable super-twisting sliding mode approach," *Automatica*, vol. 50, pp. 984–988, Mar. 2014. doi: 10.1016/j.automatica.2013.12.032.
[27] D. Yibo, X. Wang, Y. Bai, and N. Cui, "Adaptive higher order super-twisting control algorithm for a flexible air-breathing hypersonic vehicle," *Acta Astronautica*, vol. 152, pp. 275–288, Nov. 2018. doi: 10.1016/j.actaastro.2018.08.010.
[28] Y. Zhang, S. Tang, and J. Guo, "Adaptive-gain fast super-twisting sliding mode fault tolerant control for a reusable launch vehicle in reentry phase," *Isa Trans.*, vol. 71, pp. 380–390, Nov. 2017. doi: 10.1016/j.isatra.2017.08.012.
[29] M. Maryam and H. Karimpour, "Adaptive super twisting vibration control of a flexible spacecraft with state rate estimation," *J. Sound Vibrat.*, vol. 422, pp. 300–317, May 018. doi: 10.1016/j.jsv.2018.02.037.
[30] Z. Guo, J. Chang, J. Guo, and J. Zhou, "Adaptive twisting sliding mode algorithm for hypersonic reentry vehicle attitude control based on finite-time observer," *Isa Trans.*, vol. 77, pp. 20–29, Jun. 2018. doi: 10.1016/j.isatra.2018.04.001.
[31] H. Pan, X. Jing, and W. Sun, "Robust finite-time tracking control for nonlinear suspension systems via disturbance compensation," *Mech. Syst. Signal Process.*, vol. 88, pp. 49–61, May 2017. doi: 10.1016/j.ymssp.2016.11.012.
[32] Z. Liang, C. Wei, R. Wu, and N. Cui, "Fixed-time extended state observer based non-singular fast terminal sliding mode control for a VTVL reusable launch vehicle," *Aerosp. Sci. Technol.*, vols. 82–83, pp. 70–79, Nov. 2018. doi: 10.1016/j.ast.2018.08.028.
[33] M. You, Q. Zong, B. Tian, X. Zhao, and F. Zeng, "Comprehensive design of uniform robust exact disturbance observer and fixed-time controller for reusable launch vehicles," *IET Control Theory Appl.*, vol. 12, no. 5, pp. 638–648, Mar. 2018. doi: 10.1049/iet-cta.2017.0466.
[34] C. Chen, "Research on reentry attitude control for hypersonic vehicle based on disturbance compensation," Ph.D. dissertation, Dept. Control Sci. Eng., Harbin Inst. Technol., Harbin, China, 2018.
[35] K. Wu, Z. Zhang, and C. Sun, "Disturbance-observer-based output feedback control of non-linear cascaded systems with external disturbance," *IET Control Theory Appl.*, vol. 12, no. 6, pp. 738–744, Apr. 2018. doi: 10.1049/iet-cta.2017.0612.
[36] Z. Wang and Z. Wu, "Six-DOF trajectory optimization for reusable launch vehicles via Gauss pseudospectral method," *J. Syst. Eng. Electron.*, vol. 27, no. 2, pp. 434–441, Apr. 2016. doi: 10.1109/JSEE.2016.00044.

Authors' photographs and biographies not available at the time of publication.